


RESEARCH ARTICLE

Second messenger molecules have a limited spread in olfactory cilia

Hiroko Takeuchi  and Takashi Kurahashi

Odorants are detected by olfactory receptors on the sensory cilia of olfactory receptor cells (ORCs). These cylindrical cilia have a diameters of 100–200 nm, within which the components required for signal transduction by the adenylyl cyclase–cAMP system are located. The kinetics of odorant responses are determined by the lifetimes of active proteins as well as the production, diffusion, and extrusion/degradation of second messenger molecules (cAMP and Ca²⁺). However, there is limited information about the molecular kinetics of ORC responses, mostly because of the technical limitations involved in studying such narrow spaces and fine structures. In this study, using a combination of electrophysiology, photolysis of caged substances, and spot UV laser stimulation, we show that second messenger molecules work only in the vicinity of their site of generation in the olfactory cilia. Such limited spreading clearly explains a unique feature of ORCs, namely, the integer multiple of unitary events that they display in low Ca²⁺ conditions. Although the small ORC uses cAMP and Ca²⁺ for various functions in different regions of the cell, these substances seem to operate only in the compartment that has been activated by the appropriate stimulus. We also show that these substances remain in the same vicinity for a long time. This enables the ORC to amplify the odorant signal and extend the lifetime of Ca²⁺-dependent adaptation. Cytoplasmic buffers and extrusion/degradation systems seem to play a crucial role in limiting molecular spreading. In addition, binding sites on the cytoplasmic surface of the plasma membrane may limit molecular diffusion in such a narrow space because of the high surface/volume ratio. Such efficient energy conversion may also be broadly used in other biological systems that have not yet been subjected to systematic experiments.

Introduction

Olfaction starts at the sensory cilia of olfactory receptor cells (ORCs). This site mediating the sensory transduction exhibits a fine cylindrical structure with a diameter of 100–200 nm and a length of several 10s of micrometers (Usukura and Yamada, 1978; Lidow and Menco, 1984). All elements needed for signal conversion are found here: olfactory receptor protein, G protein, adenylyl cyclase, and cyclic nucleotide-gated (CNG) and Ca²⁺-activated Cl (Cl_(Ca)) channels. Through signal transduction, cAMP and Ca²⁺ play central roles as second (and third) messengers within a narrow space (Schild and Restrepo, 1998; Kaupp and Seifert, 2002; Kleene, 2008; Frings, 2009). Therefore, the kinetics of the odorant response is determined by the lifetimes of active forms of proteins and the production, diffusion, and extrusion/degradation of second messenger molecules.

So far, however, there is limited information regarding the time course of active second messengers, mostly because of experimental difficulties involved in studying such narrow spaces and fine structures. Moreover, several features of olfac-

tory responses have not yet been clarified. For instance, how the Ca²⁺-dependent adaptation of odorant response stays for >10 s (Kurahashi and Menini, 1997), whereas the normal diffusion of Ca²⁺ is much faster than such a time course (e.g., Wang, 1952, $D = 770 \mu\text{m}^2/\text{s}$; Hodgkin and Keynes, 1957; Blaustein and Hodgkin, 1969, $600 \mu\text{m}^2/\text{s}$) has been a long-standing mystery. In this study, we investigated the spatial and temporal dynamics of second messenger molecules. First, cAMP movement was monitored by observing the response time course and response summations when cytoplasmic cAMP locally and transiently jumped in the cilium. Second, the dynamics of Ca²⁺ was monitored by observing the adaptation that is exclusively regulated by Ca²⁺ feedback to the transduction system (Matthews and Reisert, 2003; Trudeau and Zagotta, 2003; Kleene, 2008). We recognized that molecules worked only in the vicinity of the site of generation in cilia with limited spreading and were present for a long time in the same area. These properties may be responsible for extending the olfactory signal to a brief pulse and for holding the adaptation for

Department of Biophysical Dynamics, Graduate School of Frontier Biosciences, Osaka University, Suita, Osaka, Japan.

Correspondence to Hiroko Takeuchi: hiroko@fbs.osaka-u.ac.jp.

© 2018 Takeuchi and Kurahashi This article is distributed under the terms of an Attribution–Noncommercial–Share Alike–No Mirror Sites license for the first six months after the publication date (see <http://www.rupress.org/terms/>). After six months it is available under a Creative Commons License (Attribution–Noncommercial–Share Alike 4.0 International license, as described at <https://creativecommons.org/licenses/by-nc-sa/4.0/>).

a longer time than when regulated using freely diffusible molecules. This finding also provided information regarding the strong polarization of ORCs. Although these compact cells use cAMP and Ca^{2+} commonly in a variety of functions in different parts, these two substances seem to work only in the compartment that generated them with appropriate stimuli. Cytoplasmic buffers and extrusion/degradation may play a crucial role in limiting substance spreading. In addition, there is a possibility that because of a high surface/volume ratio, binding sites in the cytoplasmic surface of the plasma membrane may limit molecular diffusion in such a narrow space.

Materials and methods

Cell dissociation

ORCs were dissociated enzymatically from the olfactory epithelium of newts (*Cynops pyrrhogaster*) as described previously (Kurahashi, 1989, 1990; Takeuchi and Kurahashi, 2002, 2005, 2008). The experiments were performed in compliance with the latest ethical guidelines for animal experimentation at Osaka University based on international experimentation regulations. The animals were anesthetized by cooling and then were double-pithed. After decapitation, the olfactory epithelia were removed and incubated (37°C for 5 min) in a 0.1% collagenase solution with a Ca^{2+} - and Mg^{2+} -free condition containing (in mM) 110 NaCl, 3.7 KCl, 10 Hepes, 15 glucose, 1 pyruvate, and 0.0005% phenol red, pH 7.4. Single cells were mechanically isolated. Cells were put on concanavalin A-coated glass-bottom culture dishes and bathed in normal Ringer's solution containing (in mM) 110 NaCl, 3.7 KCl, 3 CaCl_2 , 1 MgCl_2 , 10 Hepes, 15 glucose, and 1 pyruvate, plus 0.0005% phenol red. We chose cells whose cilia tightly adhered to the bottom of the dish. All experiments were performed at room temperature ($23\text{--}25^{\circ}\text{C}$).

Electrophysiology

Ciliary currents were monitored with the whole-cell (WC) recording configuration (Hamill et al., 1981; Takeuchi and Kurahashi, 2008). The membrane potentials were corrected for by the liquid junction potential at the pipette tip (4 mV; Kurahashi, 1989). The culture dish was mounted on a laser scanning microscope (LSM 510, Axiovert 200M; Zeiss) for local photolysis or a Nikon TMD for diffuse UV photolysis. Patch pipettes (resistance 10–15 M Ω) were made of borosilicate tubing (Takeuchi and Kurahashi, 2002, 2003; Takeuchi et al., 2009, 2013). The recording pipette was, unless otherwise indicated, filled with a Cs solution (in mM): 119 CsCl, 1 CaCl_2 , 5 EGTA, 10 Hepes, 0.0005% phenol red, and 1 caged cAMP (EMD Millipore). For caged Ca experiments, 1 mM CaCl_2 and 3 mM DM-nitrophen (EMD Millipore) were added to a pipette solution containing (in mM) 119 CsCl, 10 Hepes, and 0.0005% phenol red without adding EGTA. Data were sampled with pClamp v.10 (Molecular Devices) at 10 kHz after low-pass filtering at 2 kHz. For curve drawings, data were low-pass fast Fourier transformation-filtered at 0.02 kHz. Throughout the cell experiments, the holding voltage was -54 mV with correction for junction potentials, and care was taken to not cause saturation of response, especially when we looked at the amplification and/or adaptation.

The results were analyzed by an offline computer and plotted using Microcal Origin 8.6 software (OriginLab). For curve drawings, data sampled at 1/16 kHz were used in whole cilia experiments. Data are presented as mean \pm SD for the number of experiments indicated. The unpaired *t* test in Origin software was used for Fig. 2 D (normal and 0 Ca^{2+}) as well as Fig. 2 (E and F).

Photolysis of caged compound in cilia

Caged cAMP was dissolved in DMSO (Takeuchi and Kurahashi, 2002, 2005, 2008), and caged Ca was dissolved in 10 mM CsOH (Takeuchi et al., 2009, 2013). Both stock solutions were then stored at -20°C in complete darkness for up to 180 d. Before each experiment, the stock was diluted to a Cs solution as described above. After the establishment of the WC recording configuration, caged compounds were introduced to the cell interior by free diffusion.

The whole cilia of an ORC were stimulated with an epifluorescent UV system as previously reported (Takeuchi and Kurahashi, 2002). The UV component from a 100-W xenon lamp was used as the UV source. A computer-regulated magnetic shutter controlled the timing and duration of the UV light. The light intensity was set by a neutral-density wedge filter that was controlled by a pulse motor.

For local uncaging on a single cilium, we used the LSM system as previously reported (Takeuchi and Kurahashi, 2008). An 80-mW UV laser beam (argon laser, $\lambda = 351, 364$ nm; Coherent) was used for the photolysis. Throughout the experiments, the UV intensity was regulated by the transmission parameter of an acousto-optic tunable filter device. The region of interest (ROI) function of the LSM system was used for the spatially restricted stimulation as mentioned previously (Takeuchi and Kurahashi, 2008). Colored indicators in figures show the 2D image of light strength constructed by the Gaussian laser beam. The ROI-selected edge corresponds with 50% intensity. Red in the indicator represents 99–100%; orange, 75–99%; yellow, 50–75%; green, 25–50%; and blue, 0.02–25% (Takeuchi and Kurahashi, 2008). The laser beam moves on the *x* and *y* axes with the raster scan. During the current recording, the timing and duration of the actual laser irradiation were detected using a UV-photodiode (G6262; Hamamatsu Photonics). Because the sensitivity of the G6262 photodiode to the UV component transmitted via the optical fiber for the UV region was still low, a 488-nm laser was added for detection. This 488-nm laser beam alone did not cause photolysis when examined with cells. For double-pulse stimulation, we continuously used the scan mode and bleach mode.

Local double-pulse protocol

Movements of cAMP and Ca^{2+} along the ciliary cytoplasm were monitored based on the current amplification and adaptation, respectively (Fig. 1, A and B). The nonlinear summation caused by cytoplasmic cAMP has quantitatively been well described (Lowe and Gold, 1993; Takeuchi and Kurahashi, 2003). The ciliary adaptation is completely abolished when external Ca^{2+} is omitted (Kurahashi, 1990) or when a strong Ca^{2+} chelator is introduced into the cytoplasm (Kurahashi and Shibuya, 1990). Furthermore, it has been broadly known that Ca^{2+} entry through the CNG channel regulates a feedback modulation of CNG channel

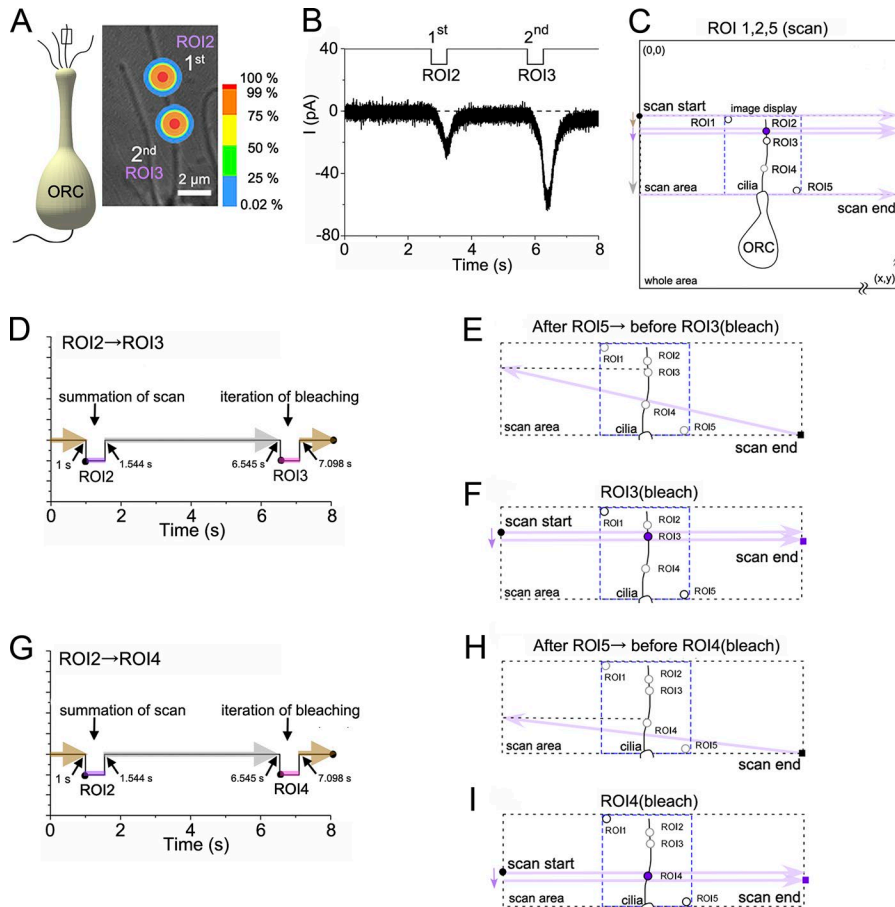


Figure 1. **Double-pulse UV stimuli to a single olfactory cilium by the LSM system.** (A) Photograph of a single cilium superimposed with the location of double stimuli. (B) Waveform of current responses and double-pulse stimulation. (C) Example of sequential stimulations at two ROIs. (D) Timing of light and scan movement (ROI2 to ROI3). (E) Movement of laser position after ROI5 stimulation to ROI3 stimulation. (F) Movement to ROI3. (G) Timing of light and scan movement (ROI2 to ROI4). (H) Movement after ROI5 before ROI4 stimulation. (I) Movement during ROI4.

(Kurahashi, 1990; Kurahashi and Shibuya, 1990; Chen and Yau, 1994; Balasubramanian et al., 1996; Kurahashi and Menini, 1997; Leinders-Zufall et al., 1997; Kleene, 1999; Bradley et al., 2001, 2004; Munger et al., 2001; Boccaccio et al., 2006; Stephan et al., 2011; De Palo et al., 2012; Li et al., 2016). To obtain spatial information, we used sequential double short-pulse UV stimuli at two distinct points along a single cilium (Fig. 1, A and B). Short-pulse (<1-s) stimulations were used because in such conditions, adaptations are mainly controlled by a Ca^{2+} feedback to the CNG channel (Kurahashi and Menini, 1997). With long and step stimulations, other mechanisms may be added to the adaptive phenomenon (e.g., Leinders-Zufall et al., 1999).

When a conventional raster scan in the LSM system was used, the interstimulus interval varied depending on the distance between the two stimulus points (Fig. 1 C). To fix the parameters, in this study, we set five ROIs in the scan image (ROI1–5; Fig. 1, C, E, F, H, and I). The y axis of ROI1 was designated as the upper limit (\bullet , x_0 , y_{ROI1}), and that of ROI5 as the lower limit (\blacksquare , x_{ROI5} , y_{ROI5}) of the scan, both of which were set outside of the cilium. The first UV stimulation was applied at ROI2 with a time series (scan) mode in LSM510. ROI3 was the second stimulus point with a short distance and ROI4 with a longer distance.

During the raster scan, the position of the laser beam moved unidirectionally from the left to the right (Fig. 1 C, right purple arrows) and from the top to the bottom in the scan area (Fig. 1, C, E, F, H, and I, black dotted area). The scan time was determined by the scan speed (pixel dwell) and the position of the ROIs (co-

ordinates x and y; Fig. 1, C, E, F, H, and I, blue dotted area). The laser was switched on only when it positioned itself at the ROI.

Fig. 1 (D–F) shows a double-pulse protocol with ROI2 and ROI3. During the first scan, ROI1, ROI2, and ROI5 were illuminated by the UV laser beam, but among them, ROI1 and ROI5 were unrelated to the stimulus to the cilium. The dark yellow arrow indicates the delay from the start of scan (Fig. 1, C, D, and G). After ROI2 was illuminated, the position of the laser system moved to the end of scan area with the raster scan (Fig. 1, C and E, \blacksquare). Immediately, the laser position moved to the y axis of ROI3 (purple arrow in Fig. 1 E). After the scan started from \bullet (x_0 , y_{ROI3}), ROI3 was illuminated by UV (Fig. 1 F, inside of purple full circle). The sum of time from ROI2 to the terminal point and the scan time from \bullet (x_0 , y_{ROI3}) to ROI3 equaled the interstimulus interval of the double-pulse protocols in Fig. 1 D (gray arrow).

To extend the distance between two ROIs, we set ROI4 instead of ROI3 as the second stimulus position (Fig. 1 G). After ROI2 was illuminated and the laser beam reached the terminal, the laser position returned to the y axis of ROI4 (Fig. 1 H, purple arrow), and then ROI4 was illuminated (Fig. 1 I, inside of purple full circle). With these protocols, the interstimulus intervals between double pulses (ROI2–ROI3 and ROI2–ROI4) were kept constant, although the distances of ROIs were different. A slight time difference between the processes (ROI5 to the position of ROI3 and ROI5 to the position of ROI4) could be ignored in the experimental time resolution.

Ca imaging in a capillary

To visualize the change in $[Ca^{2+}]_i$ in the glass capillary, Fluo-4 was used as a Ca^{2+} indicator. Fine glass capillaries were made of borosilicate tubing with a filament (outer diameter, 1.5 mm; Hilgenberg GmbH) by using an electrode puller designed for making the fine pipette to be used for intracellular recording (P2; Narishige Scientific Instruments). The LSM system equipped with a Fluor (differential interference contrast) 100 \times /1.3-NA (oil immersion) objective lens and an argon laser beam ($\lambda = 458$ nm; Coherent) was used for visualization of $[Ca^{2+}]_i$ by Fluo-4. Fluo-4 was dissolved in DMSO and stored at $-20^\circ C$ under complete darkness. The stock was diluted by a Cs pipette solution including 3 mM DM-nitrophen, 1 mM $CaCl_2$, and 0 EGTA before each experiment, and the solution was put into the fine pipette. The pipette was then set on the holder of a micromanipulator, and the pipette tip was slowly approached onto the glass coverslip that formed the bottom of a Petri dish filled with normal Ringer's solution. The tip region of the pipette was bent along the surface of the coverslip such that the tip-to-taper region was situated uniformly on the focal plane. Argon lasers ($\lambda = 351, 364$ nm; Coherent) in LSM were used for photolysis.

Digital random walk with membrane-binding site

Molecular diffusions in the absence and presence of binding sites on the cytoplasmic site of the plasma membrane were simulated using a digital model coded in Microsoft Visual Basic.NET 2008. A pixel imitating a single molecule situated in 3D space randomly moved (Random function in VB.net) within a long pipe that imitated a cilium or neuronal process; the diameter of the pipe was variable. In one time step, the pixel could randomly choose 1 of 27 pixels (3D) present at and surrounding the current position. A single step was defined as 10 nm. Therefore, the spatial resolution with this model was 20-nm cubes. On the cytoplasmic surface of the plasma membrane, the pixel could proceed only to the free space without penetrating the membrane. In the model, the pipe actually had a square shape in the cross section, but the walking distance from the center to the edge was the same for any angle. Therefore, the shape of the pipe was equivalent to a circular cylinder. The time resolution of the step movement was determined by the computer clock, but the theoretical time was inversely and statistically obtained from the relation between the time and variance (σ^2) of the moving distance. Initially, the time was defined such that the global molecular movements become $\sim 250 \mu m^2/s$ (σ^2/s). Data for D were precisely obtained after execution of tasks. When the membrane had binding sites, the pixel stayed on the cytoplasmic surface of the plasma membrane for a preconditioned period, which was equivalent to the bound time (stickiness).

Results

Response time course and recovery from adaptation

We roughly estimated spatiotemporal dynamics of second messengers in cilia from the odorant- and cAMP-induced responses in the current response obtained with the WC recording configuration (Fig. 2 A). Mainly, cAMP reduction was estimated from the off-kinetics of the odorant- and cAMP-induced responses,

especially when Ca^{2+} -dependent adaptation and the Cl^- component were omitted in 0-added Ca^{2+} conditions (Kurahashi, 1989). Ca^{2+} dynamics was estimated from the time course of the Ca^{2+} -induced current and recovery from the adaptation.

Even with a brief pulse (e.g., 100 ms) of odorant or cAMP, we found that the response lasted for several seconds (see also Takeuchi and Kurahashi, 2002). In extreme cases, the lifetime was >10 s (Fig. 2 B; see also Kurahashi, 1989; Takeuchi and Kurahashi, 2002). If cAMP diffused freely, the cytoplasmic cAMP concentration in the cilia would drop immediately, owing to molecular diffusion from the proximal part of cilia to the dendrosomatic area. It has been known that one-dimensional cAMP diffusion is considerably rapid. The SD calculated from its diffusion coefficient (D_{cAMP}) is $19 \mu m/s$ ($D_{cAMP} = 270\text{--}370 \mu m^2/s$; Chen et al., 1999); the value is already longer than the total length of newt olfactory cilia ($\sim 10 \mu m$). D_{Ca} is very similar to D_{cAMP} as described earlier.

Furthermore, we found that the lifetimes of cAMP- and Ca^{2+} -induced responses were gradually prolonged during recordings after the establishment of the WC recording configuration (Fig. 2, B and C). The half decay time of the cAMP-induced response was 0.18 ± 0.12 s ($n = 3$) 3 min after the establishment of the WC recording configuration (Fig. 2 D [black circles] and Fig. 2 E) and 0.18 ± 0.10 s ($n = 7$) for the Ca^{2+} -induced current (Fig. 2 F). At 13 min, half decay times of the cAMP- and Ca^{2+} -induced current responses induced by photolysis were 2.05 ± 2.04 s ($n = 4$) and 1.09 ± 0.64 s ($n = 5$), respectively (Fig. 2 D [black circles] and Fig. 2, E and F). We do not know the precise mechanism of the response prolongation during recordings (see Discussion). However, the result strongly suggests that both cAMP and Ca^{2+} are present in cilia for such a long time.

When $[Ca^{2+}]_o$ was reduced, the half decay time was significantly prolonged, even immediately after the establishment of the WC recording configuration (3 min in Fig. 2 D; white circles). It has been reported that odor responses are prolonged in time course when the external Ca^{2+} is removed (Kurahashi, 1989) or when the membrane is held at positive potentials in which Ca^{2+} influx is reduced (Takeuchi and Kurahashi, 2002, 2003). One of the obvious reasons for the extension was that the adaptation was lowered in these conditions. The short-term adaptation in the olfactory cilia is regulated by the influx of Ca^{2+} that passes through the CNG channel (Kurahashi, 1990; Kurahashi and Shibuya, 1990; Chen and Yau, 1994; Balasubramanian et al., 1996; Kurahashi and Menini, 1997; Leinders-Zufall et al., 1997; Kleene, 1999; Bradley et al., 2001, 2004; Munger et al., 2001; Boccaccio et al., 2006; Stephan et al., 2011; De Palo et al., 2012; Li et al., 2016). This adaptation is almost completely abolished when the Ca^{2+} feedback to the transduction machinery stops (Kurahashi, 1990; Kurahashi and Shibuya, 1990).

In addition, the response was prolonged gradually during the recording even in the 0-added Ca^{2+} media (Fig. 2 D, white circles). Such a time-dependent prolongation cannot be explained by the reduction of Ca^{2+} -dependent adaptation. The results again suggest that cAMP and Ca^{2+} stay in cilia longer than free diffusional processes (see also below). Similarly to this study, experiments using the suction pipette recording that does not affect cytoplasmic factors have shown that the odorant response lasts for >5 s in

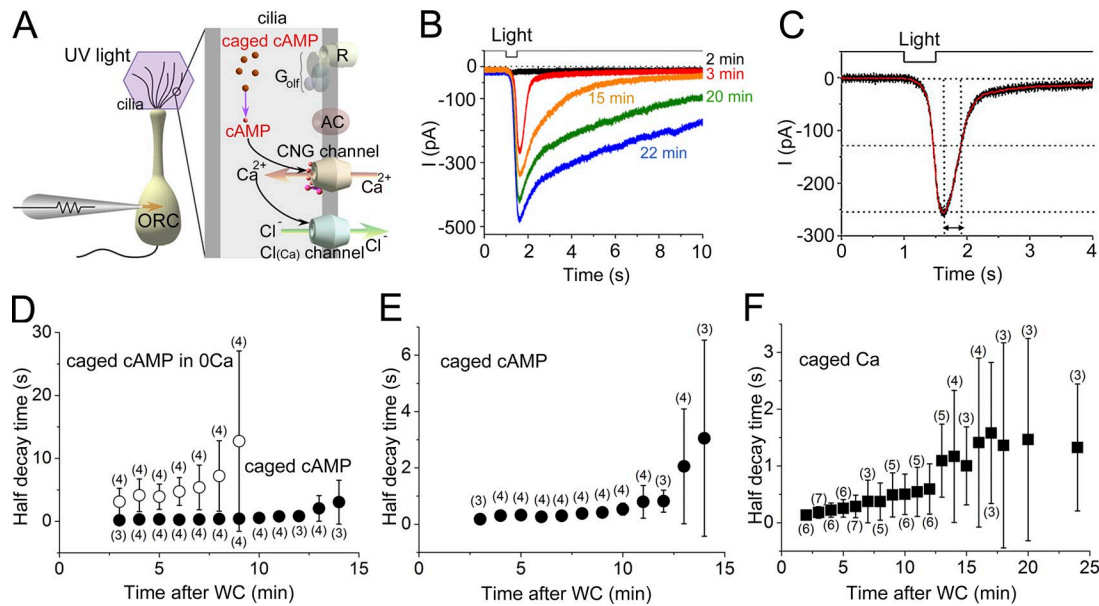


Figure 2. Decay time courses of the cAMP-induced and Ca²⁺-induced current. (A) Scheme of the transduction cascade and UV photolysis of caged cAMP. Cytoplasmic caged cAMP was photolysed using the UV light applied from a conventional photolysis system equipped with a xenon lamp. Diffuse light was applied to the entire cilia. (B) Light-induced current responses after the establishment of the WC recording configuration. Extracellular solution and normal Ringer's solution. (C) Measurement of half decay time (arrow) in a cAMP-induced current 3 min after the establishment of the WC recording configuration. (D) Change of the half decay time of cAMP responses during the WC recording. Half decay times are plotted against the time after the establishment of WC recording configuration. ●, data in normal Ca²⁺ condition; ○, data in the absence of Ca²⁺. Error bars indicate SD. Numbers in parentheses are the numbers of cells examined. Statistical significances (unpaired *t* test, *P* < 0.05) were recognized between ● (normal) and ○ (0 Ca²⁺) when examined at the same time points. (E) Expanded plot of data in normal Ca²⁺ conditions. Same data as in D. (F) Change of half decay time of caged Ca response after the establishment of the WC recording. No statistical significances (unpaired *t* test, *P* < 0.05) were recognized between E and F when examined at the same time points.

the absence of external Na⁺ (in these conditions, Ca²⁺ extrusion by Na⁺/Ca²⁺ exchange is reduced; Reisert and Matthews, 2001). The long-lasting response could presumably be due to the continuous activation of the Cl⁻ channel by cytoplasmic Ca²⁺. Therefore, it seems likely that Ca²⁺ stays within cilia for a long time even when cytoplasmic factors are not manipulated.

Double-pulse stimuli at two tiny areas within the single cilium

In a previous work (Takeuchi and Kurahashi, 2008), we applied double-pulse stimuli at two distinct points within a single olfactory cilium. The second response induced at the second region was not affected by the presence of a preceding stimulus at the first region, which was applied a few micrometers away from the second region. This suggested that second messenger molecules do not travel such a distance. However, the result could even be explained when the cAMP-mediated response summation and Ca²⁺-dependent adaptation canceled each other. To discriminate between two possibilities, in this study, we stimulated two different tiny areas successively with varied distances (for methods, see Fig. 1).

A certain part of a single cilium (or two close areas) was selected with an ROI and stimulated twice successively with the photolysis of caged cAMP (Fig. 3 A). We observed two opposite effects in the secondary responses; increments (Fig. 3, A-F) and reductions (Fig. 4, A-F). Response increments were considered the nonlinear summation of responses caused by the presence of basal cAMP as documented in detail in the past (Lowe and Gold, 1993; Takeuchi and Kurahashi, 2003, 2008). In contrast,

the response reductions represented Ca²⁺-dependent adaptation (Kurahashi and Menini, 1997; Takeuchi and Kurahashi, 2003), indicating that Ca²⁺ travels to the secondary-stimulated region. Again, it is important to note that the adaptation is almost completely abolished upon omission of the Ca²⁺ feedback (Kurahashi, 1990; Kurahashi and Shibuya, 1990).

We systematically confirmed the appearance of either summation or adaptation by monitoring the change in the secondary response when the stimulus strength for the first region was varied (Fig. 3). We interpreted the response as the summation of [cAMP]_i, when the secondary response increased as the first response increased (Fig. 3, E and F) and as adaptation when the secondary response reduced as the first response increased (Fig. 4, A-F). Of 12 ORCs, six showed summation and three showed adaptation, whereas three ORCs showed neither summation nor adaptation, whereas three ORCs showed neither summation nor adaptation may indicate the absence of the function and/or spreading of second messengers. At the same time, it is possible that in these cells, adaptation and summation may have compensated for each other. These matters were not analyzed further in this study.

It was puzzling to see that depending on the sample, either of these two phenomena became dominant. Presumably, this represented the complex mixture of several factors that include differences in cell conditions (basal concentration of second messenger molecules), double-pulse interval, distance of ROIs, variation of buffering and extrusion/degradation systems, and other parameters. At this moment, we are unable to describe their causes systematically.

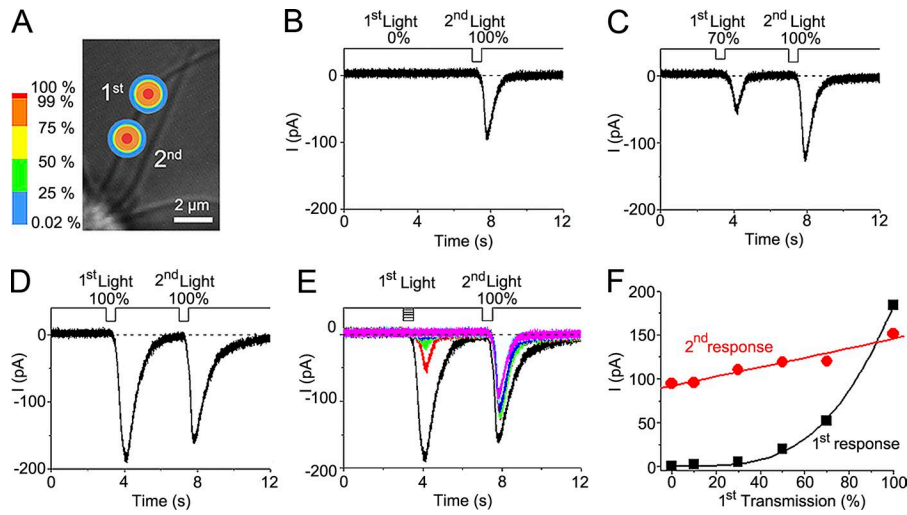


Figure 3. Example of response summation. (A) Photograph of cilia and positions of the first and the second stimulation area (ROIs). Diameter of ROIs was 1.5 μm (50% in the color scale). (B) Current responses obtained with double-pulse stimulation. First transmission of acousto-optic tunable filter device (proportional to the strength of the stimulus), 0%; second transmission, 100%. (C) First transmission, 70%; second transmission, 100%. (D) First transmission, 100%; second transmission, 100%. (E) Superimposed data from B–D and additional experiments. First transmission, 70%, 50%, 30%, 10%, and 0%. (F) Dose–response relation. The amplitudes of inward currents were plotted for both first and second responses against transmissions used for the first stimuli. \blacksquare , first response; \bullet , second response. Data from E. In this cell, the response induced at a proximal part (second in A) was smaller than that induced at a distal position (first in A), which is unusual because the response is generally bigger at the proximal part. There is a possibility that the edge of the first stimulus also stimulated the neighboring cilium.

After the identification of summation or adaptation, we changed the distance between two ROIs. Because the summation was caused by cAMP and adaptation by Ca^{2+} , such experiments can investigate the cAMP and Ca^{2+} spreading (Fig. 5, A–I). As positions of ROIs were changed, the summation and adaptive effects were reduced and became undetectable at $\sim 2\text{--}3\ \mu\text{m}$ (Fig. 5 J). The result indicated that spreading of cAMP and Ca^{2+} that are effective in physiological functions in the cilium is restricted within this distance.

So far, molecular spreading in a single cilium was investigated within relatively small time window (e.g., $<10\ \text{min}$) after the establishment of the WC recording configuration. Under such conditions, apparent spreading was found to be limited within 2–3- μm distance (Fig. 5 J). We also checked whether such limitation was kept for a long time during the recording because in a longer time window, soluble factors are assumed to be washed out from the cytoplasm. Especially, we examined the relation between a change in the current shape and the distance between two ROIs and the

time after the rupture of patch membrane (Fig. 6 A). The current ratio was obtained as the ratio between the second response after the first stimulus and second response only (Fig. 6, B–E). We did not observe any cells in which the second response reduced with the presence of the first response. Therefore, it seemed likely that the adaptation was abolished in such conditions (Fig. 6 F). In two cells (violet and indigo bars in Fig. 6 F), cAMP spreading that was estimated from the summation of responses was again reduced at distance $>2\ \mu\text{m}$, even after 25 min. Interestingly, however, we could observe in a cell (pink bar) that cAMP spreading was recognized as a response summation even at two stimulating points $>2\ \mu\text{m}$, which was not observed at the early time window during the WC recording. The results suggested that soluble factors (Ca-CAM, Song et al., 2008, and/or phosphodiesterase [PDE]) are, at least in part, involved in the limitation of spreading because prolongation of the cAMP-induced response can at least be explained by the washout (and/or dysfunction) of such factors.

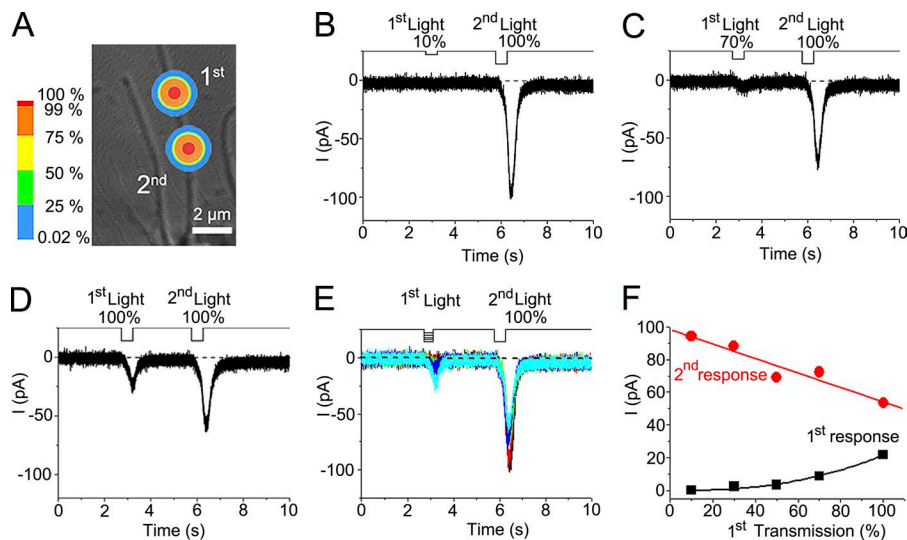


Figure 4. Example of response reduction. (A) Photograph of cilia and positions of two ROIs (the first and the second). Diameter of ROIs was 1.5 μm . (B) Current responses obtained with double-pulse stimulation. First transmission, 10%; second transmission, 100%. (C) First transmission, 70%; second transmission, 100%. (D) First transmission, 100%; second transmission, 100%. (E) Superimposed data from B–D and additional experiments. First transmissions, 100%, 70%, 50%, 30%, and 10%. (F) Dose–response relation. The amplitudes of inward currents were plotted for both first and second responses against transmissions used for the first stimuli. \blacksquare , first response; \bullet , second response. Data obtained from E.

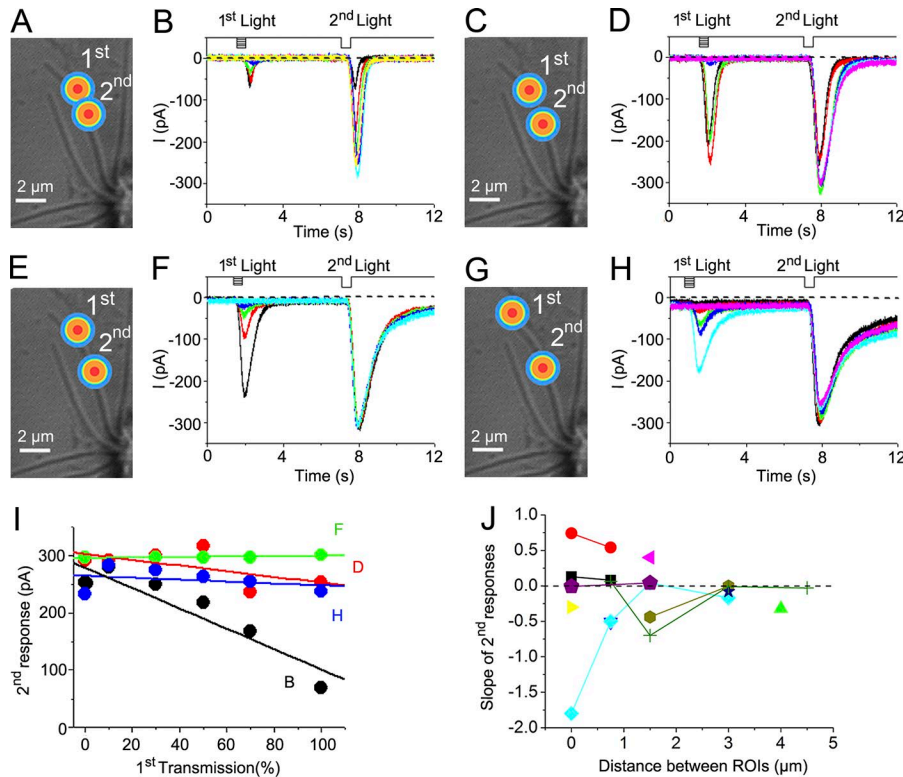


Figure 5. Effect of changed distance between two ROIs. (A) Photograph of cilia and positions of ROIs. Diameter of ROIs, 1.5 μm . Distance between the first and the second ROI was nearly 0, the distance measured at 50% intensity line. (B) Superimposed waves. First transmissions, 100%, 70%, 50%, 30%, and 10%. (C) Photograph of cilia and ROIs. Distance, 0.75 μm . (D) Superimposed waves. (E) Photograph of cilia and ROIs. Distance, 1.5 μm . (F) Superimposed waves. (G) Photograph of cilia and ROIs. Distance, 3.0 μm . (H) Superimposed waves. (I) Dose-response relation. Amplitudes of second responses were plotted against the first transmission. Data from B, D, F, and H. (J) Distance between ROIs (measured at intensity of 50%) and slope of the dose-response relations. Each symbol represents data from different cilia (different cells, $n = 12$).

Ca²⁺ diffusion in a fine glass capillary

As a control experiment, we measured Ca²⁺ diffusion in a thin glass capillary with $\sim 1\text{-}\mu\text{m}$ inner diameter. The capillary was filled with caged Ca and Fluo-4, and a local area of $\sim 1\text{-}\mu\text{m}$ diameter was illuminated by a UV laser (Fig. 7A, arrow). The Ca²⁺ signal increased immediately after irradiation, after which it decreased rapidly at the stimulus center and spread laterally along the capillary (Fig. 7B). The fluorescence distribution could be fitted by the Gaussian function (Fig. 8, A and B). By plotting σ^2 against time (Fig. 8 C), we obtained the diffusion coefficient (D) of $440 \pm 35 \mu\text{m}^2/\text{s}$ ($n = 11$), which was in good agreement with standard $D_{\text{Ca}^{2+}}$ (600 $\mu\text{m}^2/\text{s}$; Hodgkin and Keynes, 1957; Blaustein and Hodgkin, 1969). In $1.8 \pm 1.0 \text{ s}$ ($n =$

5), the fluorescence became almost undetectable, which was much faster than WC responses, especially at long-lasting WC recording, or than the time needed for recovery from the adaptation. Therefore, we again recognized that the olfactory cilia have functions to extend the lifetimes of cAMP and Ca²⁺ effects.

Digital model for the random walk in the presence of binding sites

Longitudinal spreading of second messenger molecules in the olfactory cilia is highly likely to be strongly restricted, at least in physiologically reliable concentration ranges. There are several possibilities to explain how the spreading is limited

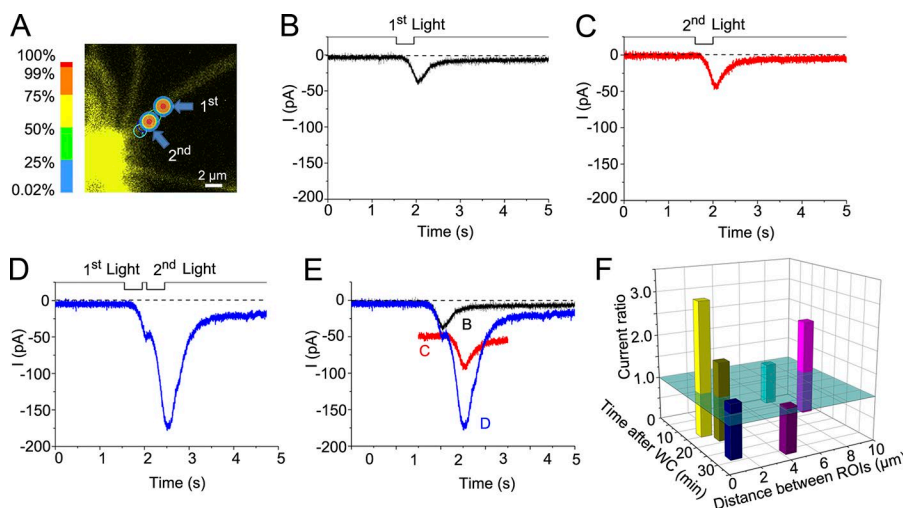


Figure 6. Spreading of cAMP after long-term WC recordings. (A) Photograph of cilia and positions of two ROIs (first and second, blue arrows). Diameter of ROIs, 1.5 μm . Distance between two ROIs, 1.3 μm . (B) Current response obtained at the first ROI. Transmission, 100%. 14 min after the establishment of the WC recording configuration. (C) Current response obtained at the second ROI. Transmission, 100%. (D) Current response obtained from double pulse stimulation, the first and the second ROIs. Transmission, 100%. (E) Superimposed current responses. Data from B–D. Note that the second response of D is augmented compared with the response shown in C. (F) Relation among distance of two ROIs (x axis), time after the establishment of the WC recording configuration (y axis), and current ratio (z axis). The current ratio was obtained as the ratio between the second response after the first stimulus and the second response only. A green level indicates current ratio = 1.0.

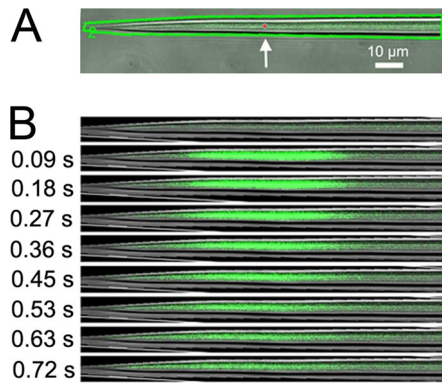


Figure 7. **One-dimensional Ca^{2+} diffusion in a fine glass capillary.** (A) Photograph of a thin glass capillary. The arrow (red point) indicates the site for photolysis of caged Ca^{2+} . A UV laser and ROI in LSM were used. The inner diameter of the pipette at the stimulus point was $0.87 \mu\text{m}$. The green area shows the scan area. Irradiation time, 92 ms. (B) Fluorescent imaging before and after photolysis. Scan time, 90 ms. Fluo-4, $100 \mu\text{M}$; DM-nitrophen, 3 mM ; CaCl_2 , 1 mM .

in the smooth tubular structure. Cytoplasmic buffers and extrusion and cAMP and Ca^{2+} degradation will be at least in part responsible for the reduction of spreading of these molecules during their diffusion. In a previous work, however, Takeuchi and Kurahashi (2008) showed that the degree of adaptation and recovery time course with a stimulus onto a confined region did not change remarkably from those observed upon the entire-cilia stimulation (Kurahashi and Menini, 1997). It is puzzling why the cAMP response and Ca^{2+} -dependent adaptation stay for $>10 \text{ s}$ even with a very confined stimulation; these molecules should quickly disappear if the rapid extrusion/degradation and buffers were the entire mechanism for restricted spreading.

We speculated that the anomalously thin structure of cilia may be responsible for the limitation of diffusional processes, mostly because of the high surface/volume ratio. In the same concentration of the solution in a cylindrical space, the binding site at the cytoplasmic surface of the plasma membrane becomes dominant to affect diffusion. To verify this possibility, we constructed a digital model that actually simulates the random walk process of molecules in the absence (Fig. 9, A and B) and presence

(Fig. 10, A and B) of binding sites on the cytoplasmic surface of the plasma membrane.

When the cytoplasmic surface did not have any binding sites, free molecules spread along the x axis (Fig. 11, A and B) and σ^2 gradually became wider with time (Fig. 11, E and F), showing a linear change in the time process (Fig. 11 I). The diffusion process was not affected by a change in the diameter when the membrane did not have binding sites (Fig. 11 J). When the membrane had binding sites that held the molecule, for example $1.16 \mu\text{m}$, D was strongly reduced (Fig. 11, C, D, G, and H). The relation between σ^2 and stickiness showed nearly an exponential decrease (Fig. 11 M). In contrast with the previous measurements, D strongly depended on the diameter of the process (Fig. 11, K and L). Plotting σ^2 against the diameter, it became obvious that diffusion actually depended on the diameter of the process when the cytoplasmic surface of the membrane had binding sites (Fig. 11 N). It is highly likely that the diffusion of soluble molecules in an anomalously fine tube like the cilium is dramatically reduced on the basis of the diameter when the cytoplasmic surface of the membrane has binding sites.

Discussion

This study showed that both cAMP and Ca^{2+} work only in the vicinity of the site of generation in the olfactory cilia. The result was consistent with the fact that ORCs show an integer multiple of unitary events observed at low Ca^{2+} conditions (Bhandawat et al., 2005), which does not occur when second messengers spread rapidly over the cilium. A similar compartmentalization has been shown in photoreceptor cells in which Ca^{2+} independently works between the outer and inner segments that are connected via a thin ciliary structure (connecting cilium; Krizaj and Copenhagen, 1998; Nair et al., 2005; Calvert et al., 2010). Some of our present findings may be related to the presence of a microdomain in the olfactory cilia (Castillo et al., 2010; Pietrobon et al., 2011; López et al., 2014; Henkel et al., 2015). In the primary cilia, Ca^{2+} signaling is also uncoupled from signaling in the cell cytoplasm (Delling et al., 2013). These findings provide examples of functional polarity in compact cells. It seems likely that the cytoplasmic buffers, extrusion systems, and degradation systems are involved in this limitation of the spreading of molecules. Additionally, it is possible that

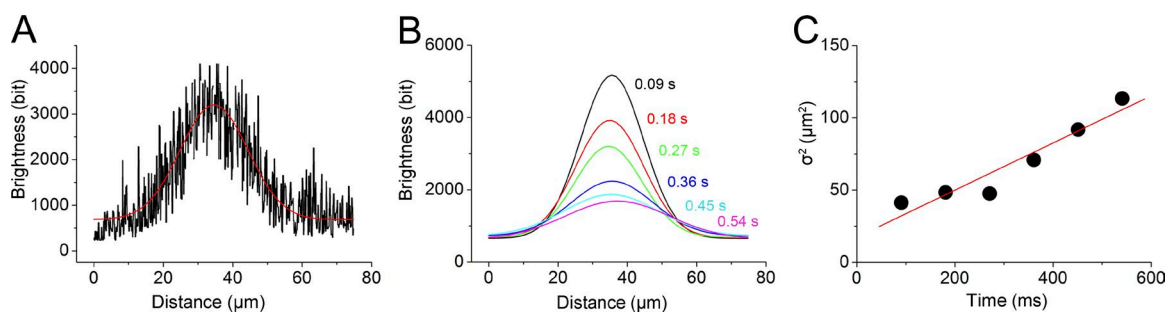


Figure 8. **Distribution and temporal change of Fluo-4 fluorescence in the fine glass capillary.** (A) Relation between the distance from the ROI and brightness 270 ms after photolysis, fitted by the Gaussian function with σ^2 of $47.6 \mu\text{m}^2$. A different capillary from Fig. 7. (B) Change in the relation between brightness and distance during the time after uncaging. Data obtained from fitting parameters in experiments as in A. (C) Relation between the time after photolysis and σ^2 . Data obtained from B. The slope gives D_{Ca} of $163.2 \mu\text{m}^2/\text{s}$ from $D = \sigma^2/2t$. We did not persist in fitting from the origin (0, 0) because UV illumination was not 0 in area. Furthermore, the glass may cause diffraction. The initiation of uncaging and emission of fluorescence may have some delay from UV irradiation.

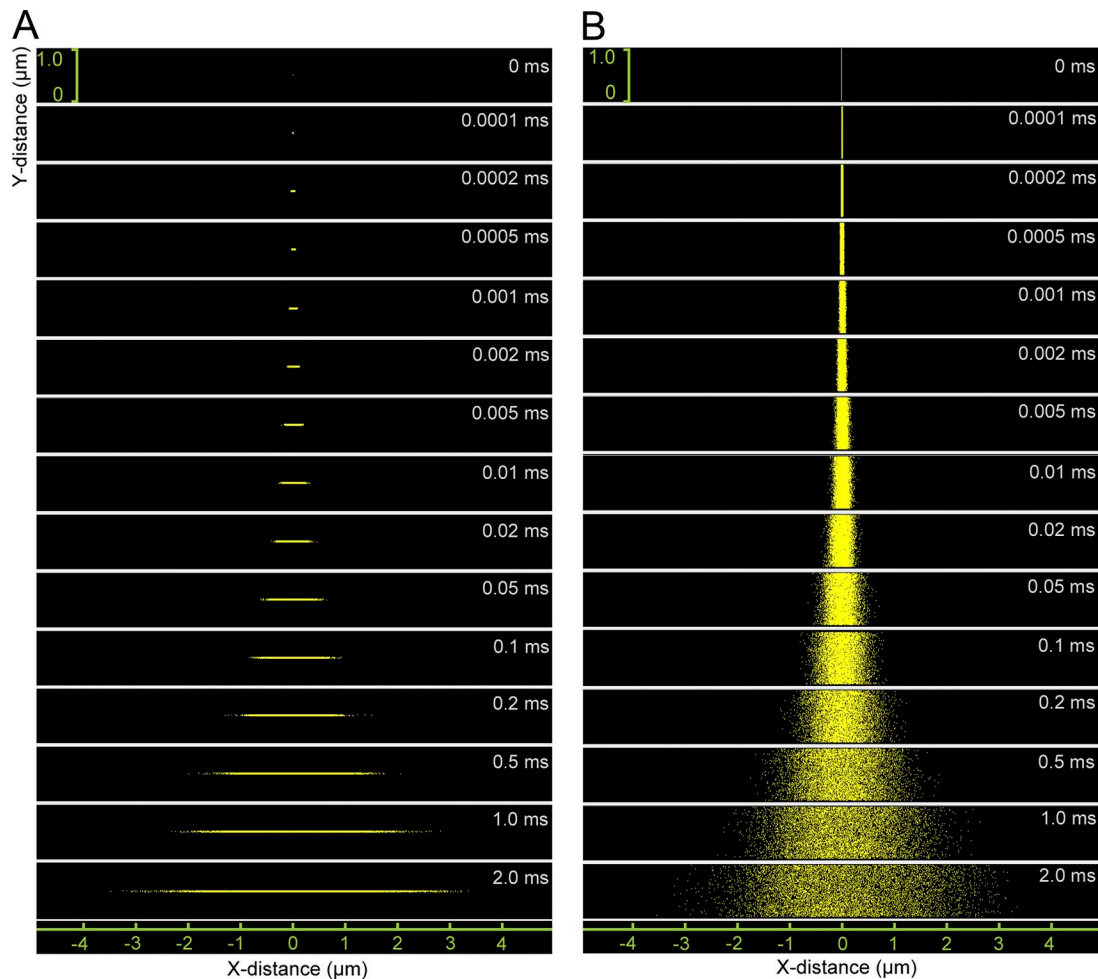


Figure 9. **Digital model for the random walk in thin and thick processes.** (A and B) Yellow dots show molecules that move independently. Number of molecules, 10,000. No binding site for molecules on the cytoplasmic surface of the membrane. At 0 ms, positions of all molecules are randomly set at the center (X distance = 0) within the size of the tube. As time progresses, the molecules laterally spread along the tube. (A) Thin process. Diameter, 0.02 μm . (B) Thick process. Diameter, 0.99 μm . Note that the diffusion process is independent of the thickness of the process.

the diffusion process strongly slows down in such a narrow space because of binding sites on the cytoplasmic surface of the plasma membrane as shown in the digital model. These properties may enable ORCs to express a long-lasting response and adaptation. The lifetime of the cAMP-induced response and recovery from adaptation were much longer than the time course for the disappearance of Ca^{2+} signals within the glass capillary. Interestingly, Ca^{2+} in the dendrosomatic region does not backpropagate into the cilia, either. The response kinetics of the odorant-induced current is unaffected by the step depolarization under the voltage clamp condition that activates voltage-gated Ca^{2+} channels located in the dendrosomatic membrane (see e.g., Kurahashi, 1989). It is also shown that Ca^{2+} signals measured with Fluo3 in the cilia did not show any sign for backpropagation of Ca^{2+} from the knob when a cilium was stimulated by an odor or the cell body was stimulated by a high K solution (Leinders-Zufall et al., 1997, 1998).

In this study, we found that the time courses of cAMP- and Ca^{2+} -induced currents prolonged during WC recordings. At this moment, the precise mechanism for this phenomenon is unknown. It is unlikely that the long-lasting WC recording configuration inhibits cAMP and Ca^{2+} diffusion in cilia; conversely, a

reduction in the activities of several factors may be involved in the prolonged time course. For instance, PDE activity is one possibility; the cAMP-dependent response is expected to be prolonged when PDE activities are lowered. Ca-CAM (Song et al., 2008) is another candidate. $\text{Na}^+/\text{Ca}^{2+}$ exchange is also reportedly involved in the response termination (Stephan et al., 2011). Furthermore, the prolongation of the Ca^{2+} response (Fig. 2 E) may be caused by a reduction of $[\text{ATP}]_i$ that is involved in Ca^{2+} extrusion (Antolin et al., 2010).

Chen et al. (1999) showed that the cAMP response of a single olfactory cilium drops within a few seconds after the washout of cytoplasmic cAMP (Chen et al., 1999). For their recording, they used a detached single olfactory cilium preparation to load and wash out cAMP from the proximal part of the cilium. In contrast, in this study, we introduced cAMP from the WC pipette situated at the dendrosomatic area. When cAMP concentration was jumped locally by photolysis of caged cAMP at the middle part of the cilium, the lifetime of the cAMP response was sometimes >10 s. There are several differences between these experimental conditions. One of the biggest differences could be the concentration of cAMP. They used $[\text{cAMP}]_i < 20 \mu\text{M}$, whereas in this study, $[\text{cAMP}]_i$ could be higher at the place of irradiation (ROI); we have

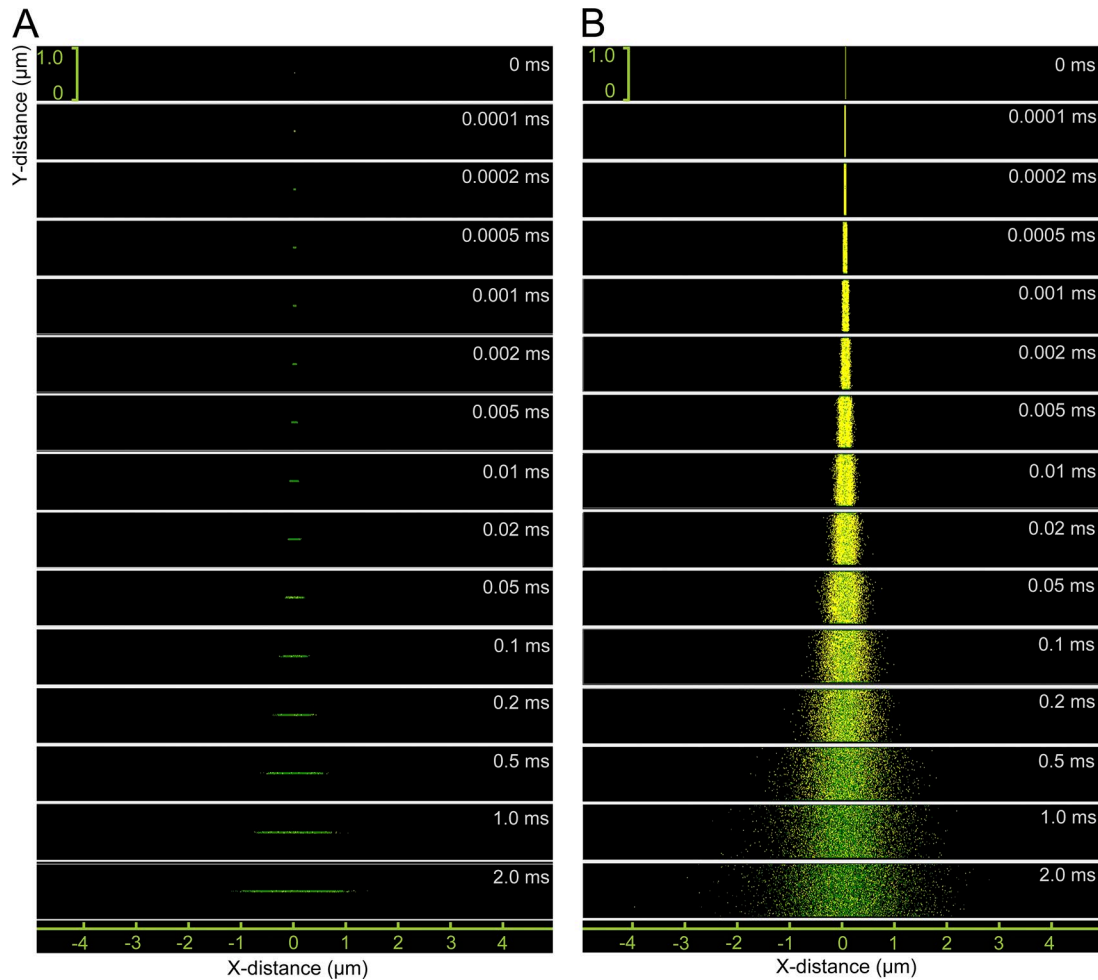


Figure 10. **Digital model for the random walk in thin and thick processes in the presence of binding sites. (A and B)** Initialization and movements of molecules are the same as those in Fig. 9 except that the cytoplasmic surface of the membrane has binding sites. Yellow dots show free molecules, and green dots indicate molecules that are bound to the membrane for the time period of 1.16 μs . Number of molecules, 10,000. **(A)** Thin process. Diameter, 0.02 μm . **(B)** Thick process. Diameter, 0.99 μm . Note that the diffusion process slows down in the thin process.

estimated that ciliary $[\text{cAMP}]_i$ could be as high as 100 μM when the cell was stimulated by odorants or caged cAMP (Takeuchi and Kurahashi, 2005). When $[\text{cAMP}]_i$ becomes high, buffering effects become dominant (Chen et al., 1999), which would slow down the diffusional processes. Moreover, cAMP and/or Ca^{2+} diffusion, the washout of cytoplasmic factors, or special distribution of voltage profiles along the cilium may have contributed to the variance. Further experiments are warranted to clarify this.

It is controversial whether cAMP that is generated in cilia upon odorant stimulation diffuses to the dendrosomatic regions (e.g., Reisert and Zhao, 2011). cAMP plays important roles in the cell body for (a) the change in the spiking properties via an A-kinase (Kawai et al., 1999), and (b) the determination of basal activity via an HCN channel (Nakashima et al., 2013) that may be related to selective axonal projection (Imai et al., 2006; Imai and Sakano, 2009; Mobley et al., 2010). Our finding regarding slow diffusion and well-known degradation in the olfactory cilia indicates that cAMP generated in the cilia does not affect cellular activities conducted at the cell body. The geometrical spatial ratio between the cilia and the dendrosomatic regions needs to be considered. The total volume of the cilia is 1 $\pi\mu\text{m}^3$ (0.2 μm

diameter and 10 μm length; 10 cilia), whereas that of dendrosomatic regions is 470 $\pi\mu\text{m}^3$ (dendrite, 1 μm diameter and 50 μm length; cell body, 14 μm diameter sphere), providing a ratio of ~ 500 . Even if there was no diffusion limitation or extrusion/degradation in cilia, 10 μM cAMP generated at cilia became 20 nM in the dendrosomatic regions (Takeuchi and Kurahashi, 2005), which is already lower than the physiologically reliable range.

This study showed that the diffusion of molecules slows down based on diameter of processes when the cytoplasmic surface of the plasma membrane has binding sites. The cytoplasmic side of the olfactory cilia has several binding sites for cAMP and Ca^{2+} (e.g., microdomain in cilia, Castillo et al., 2010). The ciliary membrane contains an anomalously high density of CNG channels (Kurahashi and Kaneko, 1991, 1993), 700–2,300 molecules of CNG channels in 1- μm length of the olfactory cilium (Kurahashi, 1990). Each CNG channel forms a tetramer, having four binding sites in individual molecules. Therefore, the binding sites for cAMP molecules are 2,800–9,200 per 1- μm length of the cilium. The cAMP concentration reaches as high as 100 μM at the maximum (Takeuchi and Kurahashi, 2005), which gives 450 molecules per 1- μm length of the cilium, much smaller than

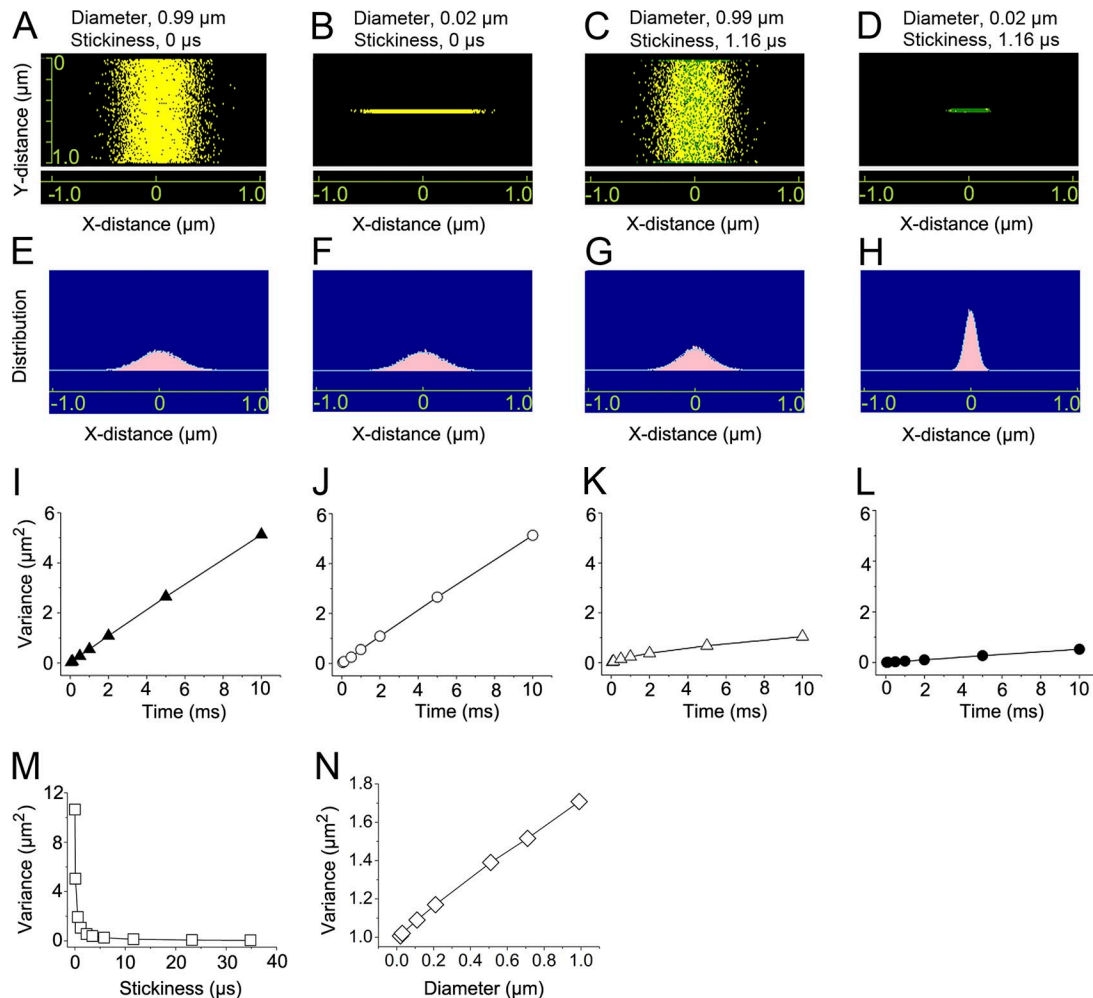


Figure 11. **Molecular diffusion in thick and thin processes in the presence and absence of binding sites.** (A–N) Relation between the movement of cytoplasmic molecules and diameter. Distributions measured at 0.058 ms. Number of molecules, 10,000. (A) Random walk of molecules in a thick process in the absence of a binding site; diameter, 0.99 μm . (B) Diameter, 0.02 μm . (C) Diameter 0.99 μm . Stickiness (the time that the molecule stays on the membrane), 1.16 μs . (D) Diameter of 0.02 μm . Stickiness, 1.16 μs . (E) Gaussian fitting of existence probability distribution of data from A. σ^2 , 0.033 μm^2 . SD, 0.18 μm . (F) Existence probability distribution of data from B. σ^2 , 0.033 μm^2 . SD, 0.18 μm . (G) Existence probability distribution of data from C. σ^2 , 0.025 μm^2 . SD, 0.16 μm . (H) Existence probability distribution of data from D. σ^2 , 0.003 μm^2 . SD, 0.06 μm . (I) Change of σ^2 in the thick process in the absence of a binding site. Diameter, 0.99 μm . Stickiness, 0. D , 256.8 $\mu\text{m}^2/\text{s}$. (J) Change of σ^2 in the thin process in the absence of a binding site. Diameter, 0.02 μm . Stickiness, 0. D , 256.1 $\mu\text{m}^2/\text{s}$. (K) Change of σ^2 in the thick process in the presence of a binding site. Diameter, 0.99 μm . Stickiness, 1.16 μs . D , 51.3 $\mu\text{m}^2/\text{s}$. (L) Change of σ^2 in the presence of a binding site. Diameter, 0.02 μm . Stickiness, 1.16 μs . D , 25.3 $\mu\text{m}^2/\text{s}$. (M) Dependence of σ^2 on stickiness. Diameter, 0.02 μm . Data were obtained with number of molecules of 1,000. Data at 20 ms. (N) Relation between the diameter and σ^2 in the presence of binding sites. Number of molecules, 1,000. Data at 20 ms. Note that σ^2 is dependent on the diameter.

the binding capacity for cAMP. With regard to the binding sites for Ca^{2+} , CaM is permanently bound to the cytoplasmic domain of each CNG channel (Chen and Yau, 1994; Bradley et al., 2001, 2004). In addition, lipid bilayers and various proteins including tubulin may serve as strong binding sites for Ca^{2+} . Besides, unidentified Ca^{2+} -binding proteins (Balasubramanian et al., 1996) and $\text{Cl}_{(\text{Ca})}$ channels (Kleene and Gesteland, 1991; Kurahashi and Yau, 1993; Reisert and Matthews, 1998) are well-known Ca^{2+} -binding sites. All of these binding sites may be responsible for limiting diffusion. Simultaneously, cAMP is degraded by PDE (Cygnar and Zhao, 2009), whereas Ca^{2+} is extruded by $\text{Na}^+/\text{Ca}^{2+}$ exchanger (Castillo et al., 2007; Stephan et al., 2011) and ATP-dependent Ca^{2+} extrusion (Antolin et al., 2010), which is involved in the restriction of molecular spreading.

For a long time, it was believed that the ciliary structure for sensory perception is responsible for the increase in the probability of stimulant capture. As the molecular dynamics were revealed, it became clear that this fine structure is quite beneficial for efficient signal transduction. As described in this study, the narrow space can limit cytoplasmic molecule diffusions, and as a result, the response becomes prolonged and adaptation lasts for a long time. The high surface/volume ratio is responsible for a rapid increase in the molecular concentration even with a low production and with a small influx of molecules. Altogether, signal transduction is achieved efficiently in such a narrow space. Such efficient energy conversion may also be broadly used in other biological systems, which have not yet been subjected to systematic experiments.

Acknowledgments

We thank Dr. Tsung-Yu Chen for valuable comments and discussions.

This study was supported by the Japan Society for the Promotion of Science KAKENHI (Grants-in-Aid for Scientific Research, C) JP16K08495 (H. Takeuchi) and JP26430016 (T. Kurahashi) and grants from international collaborating research at Osaka University (T. Kurahashi).

The authors declare no competing financial interests.

Author contributions: H. Takeuchi designed and performed cell experiments. T. Kurahashi made the simulation program and directed the project. H. Takeuchi and T. Kurahashi analyzed data and wrote the manuscript. The authors approved the final version of the manuscript.

Sharon E. Gordon served as editor.

Submitted: 13 May 2018

Revised: 12 August 2018

Accepted: 3 October 2018

References

- Antolin, S., J. Reiser, and H.R. Matthews. 2010. Olfactory response termination involves Ca^{2+} -ATPase in vertebrate olfactory receptor neuron cilia. *J. Gen. Physiol.* 135:367–378. <https://doi.org/10.1085/jgp.200910337>
- Balasubramanian, S., J.W. Lynch, and P.H. Barry. 1996. Calcium-dependent modulation of the agonist affinity of the mammalian olfactory cyclic nucleotide-gated channel by calmodulin and a novel endogenous factor. *J. Membr. Biol.* 152:13–23. <https://doi.org/10.1007/s002329900081>
- Bhandawat, V., J. Reiser, and K.W. Yau. 2005. Elementary response of olfactory receptor neurons to odorants. *Science*. 308:1931–1934. <https://doi.org/10.1126/science.1109886>
- Blaustein, M.P., and A.L. Hodgkin. 1969. The effect of cyanide on the efflux of calcium from squid axons. *J. Physiol.* 200:497–527. <https://doi.org/10.1113/jphysiol.1969.sp008704>
- Boccaccio, A., L. Lagostena, V. Hagen, and A. Menini. 2006. Fast adaptation in mouse olfactory sensory neurons does not require the activity of phosphodiesterase. *J. Gen. Physiol.* 128:171–184. <https://doi.org/10.1085/jgp.200609555>
- Bradley, J., D. Reuter, and S. Frings. 2001. Facilitation of calmodulin-mediated odor adaptation by cAMP-gated channel subunits. *Science*. 294:2176–2178. <https://doi.org/10.1126/science.1063415>
- Bradley, J., W. Bönigk, K.W. Yau, and S. Frings. 2004. Calmodulin permanently associates with rat olfactory CNG channels under native conditions. *Nat. Neurosci.* 7:705–710. <https://doi.org/10.1038/nn1266>
- Calvert, P.D., W.E. Schiesser, and E.N. Pugh Jr. 2010. Diffusion of a soluble protein, photoactivatable GFP, through a sensory cilium. *J. Gen. Physiol.* 135:173–196. <https://doi.org/10.1085/jgp.200910322>
- Castillo, K., R. Delgado, and J. Bacigalupo. 2007. Plasma membrane Ca^{2+} -ATPase in the cilia of olfactory receptor neurons: possible role in Ca^{2+} clearance. *Eur. J. Neurosci.* 26:2524–2531. <https://doi.org/10.1111/j.1460-9568.2007.05863.x>
- Castillo, K., D. Restrepo, and J. Bacigalupo. 2010. Cellular and molecular Ca^{2+} microdomains in olfactory cilia support low signaling amplification of odor transduction. *Eur. J. Neurosci.* 32:932–938. <https://doi.org/10.1111/j.1460-9568.2010.07393.x>
- Chen, T.Y., and K.W. Yau. 1994. Direct modulation by Ca^{2+} -calmodulin of cyclic nucleotide-activated channel of rat olfactory receptor neurons. *Nature*. 368:545–548. <https://doi.org/10.1038/368545a0>
- Chen, C., T. Nakamura, and Y. Koutalos. 1999. Cyclic AMP diffusion coefficient in frog olfactory cilia. *Biophys. J.* 76:2861–2867. [https://doi.org/10.1016/S0006-3495\(99\)77440-0](https://doi.org/10.1016/S0006-3495(99)77440-0)
- Cygnar, K.D., and H. Zhao. 2009. Phosphodiesterase 1C is dispensable for rapid response termination of olfactory sensory neurons. *Nat. Neurosci.* 12:454–462. <https://doi.org/10.1038/nn.2289>
- Delling, M., P.G. DeCaen, J.F. Doerner, S. Febvay, and D.E. Clapham. 2013. Primary cilia are specialized calcium signalling organelles. *Nature*. 504:311–314. <https://doi.org/10.1038/nature12833>
- De Palo, G., A. Boccaccio, A. Miri, A. Menini, and C. Altafini. 2012. A dynamical feedback model for adaptation in the olfactory transduction pathway. *Biophys. J.* 102:2677–2686. <https://doi.org/10.1016/j.bpj.2012.04.040>
- Frings, S. 2009. Primary processes in sensory cells: current advances. *J. Comp. Physiol. A Neuroethol. Sens. Neural Behav. Physiol.* 195:1–19. <https://doi.org/10.1007/s00359-008-0389-0>
- Hamill, O.P., A. Marty, E. Neher, B. Sakmann, and F.J. Sigworth. 1981. Improved patch-clamp techniques for high-resolution current recording from cells and cell-free membrane patches. *Pflugers Arch.* 391:85–100. <https://doi.org/10.1007/BF00656997>
- Henkel, B., D.R. Drose, T. Ackels, S. Oberland, M. Spehr, and E.M. Neuhaus. 2015. Co-expression of anoctamins in cilia of olfactory sensory neurons. *Chem. Senses*. 40:73–87. <https://doi.org/10.1093/chemse/bju061>
- Hodgkin, A.L., and R.D. Keynes. 1957. Movements of labelled calcium in squid giant axons. *J. Physiol.* 138:253–281. <https://doi.org/10.1113/jphysiol.1957.sp005850>
- Imai, T., and H. Sakano. 2009. Odorant receptor gene choice and axonal projection in the mouse olfactory system. *Results Probl. Cell Differ.* 47:57–75. https://doi.org/10.1007/400_2008_3
- Imai, T., M. Suzuki, and H. Sakano. 2006. Odorant receptor-derived cAMP signals direct axonal targeting. *Science*. 314:657–661. <https://doi.org/10.1126/science.1131794>
- Kaupp, U.B., and R. Seifert. 2002. Cyclic nucleotide-gated ion channels. *Physiol. Rev.* 82:769–824. <https://doi.org/10.1152/physrev.00008.2002>
- Kawai, F., T. Kurahashi, and A. Kaneko. 1999. Adrenaline enhances odorant contrast by modulating signal encoding in olfactory receptor cells. *Nat. Neurosci.* 2:133–138. <https://doi.org/10.1038/5686>
- Kleene, S.J. 1999. Both external and internal calcium reduce the sensitivity of the olfactory cyclic-nucleotide-gated channel to cAMP. *J. Neurophysiol.* 81:2675–2682. <https://doi.org/10.1152/jn.1999.81.6.2675>
- Kleene, S.J. 2008. The electrochemical basis of odor transduction in vertebrate olfactory cilia. *Chem. Senses*. 33:839–859. <https://doi.org/10.1093/chemse/bjn048>
- Kleene, S.J., and R.C. Gesteland. 1991. Calcium-activated chloride conductance in frog olfactory cilia. *J. Neurosci.* 11:3624–3629. <https://doi.org/10.1523/JNEUROSCI.11-11-03624.1991>
- Krizaj, D., and D.R. Copenhagen. 1998. Compartmentalization of calcium extrusion mechanisms in the outer and inner segments of photoreceptors. *Neuron*. 21:249–256. [https://doi.org/10.1016/S0896-6273\(00\)80531-0](https://doi.org/10.1016/S0896-6273(00)80531-0)
- Kurahashi, T. 1989. Activation by odorants of cation-selective conductance in the olfactory receptor cell isolated from the newt. *J. Physiol.* 419:177–192. <https://doi.org/10.1113/jphysiol.1989.sp017868>
- Kurahashi, T. 1990. The response induced by intracellular cyclic AMP in isolated olfactory receptor cells of the newt. *J. Physiol.* 430:355–371. <https://doi.org/10.1113/jphysiol.1990.sp018295>
- Kurahashi, T., and A. Kaneko. 1991. High density cAMP-gated channels at the ciliary membrane in the olfactory receptor cell. *Neuroreport*. 2:5–8. <https://doi.org/10.1097/00001756-199101000-00001>
- Kurahashi, T., and A. Kaneko. 1993. Gating properties of the cAMP-gated channel in toad olfactory receptor cells. *J. Physiol.* 466:287–302.
- Kurahashi, T., and A. Menini. 1997. Mechanism of odorant adaptation in the olfactory receptor cell. *Nature*. 385:725–729. <https://doi.org/10.1038/385725a0>
- Kurahashi, T., and T. Shibuya. 1990. Ca^{2+} -dependent adaptive properties in the solitary olfactory receptor cell of the newt. *Brain Res.* 515:261–268. [https://doi.org/10.1016/0006-8993\(90\)90605-B](https://doi.org/10.1016/0006-8993(90)90605-B)
- Kurahashi, T., and K.W. Yau. 1993. Co-existence of cationic and chloride components in odorant-induced current of vertebrate olfactory receptor cells. *Nature*. 363:71–74. <https://doi.org/10.1038/363071a0>
- Leinders-Zufall, T., M.N. Rand, G.M. Shepherd, C.A. Greer, and F. Zufall. 1997. Calcium entry through cyclic nucleotide-gated channels in individual cilia of olfactory receptor cells: spatiotemporal dynamics. *J. Neurosci.* 17:4136–4148. <https://doi.org/10.1523/JNEUROSCI.17-11-04136.1997>
- Leinders-Zufall, T., C.A. Greer, G.M. Shepherd, and F. Zufall. 1998. Imaging odor-induced calcium transients in single olfactory cilia: specificity of activation and role in transduction. *J. Neurosci.* 18:5630–5639. <https://doi.org/10.1523/JNEUROSCI.18-15-05630.1998>
- Leinders-Zufall, T., M. Ma, and F. Zufall. 1999. Impaired odor adaptation in olfactory receptor neurons after inhibition of Ca^{2+} /calmodulin kinase II. *J. Neurosci.* 19:RC19. <https://doi.org/10.1523/JNEUROSCI.19-14-j0005.1999>

- Li, R.C., Y. Ben-Chaim, K.W. Yau, and C.C. Lin. 2016. Cyclic-nucleotide-gated cation current and Ca^{2+} -activated Cl current elicited by odorant in vertebrate olfactory receptor neurons. *Proc. Natl. Acad. Sci. USA*. 113:11078–11087. <https://doi.org/10.1073/pnas.1613891113>
- Lidow, M.S., and B.P. Menco. 1984. Observations on axonemes and membranes of olfactory and respiratory cilia in frogs and rats using tannic acid-supplemented fixation and photographic rotation. *J. Ultrastruct. Res.* 86:18–30. [https://doi.org/10.1016/S0022-5320\(84\)90092-3](https://doi.org/10.1016/S0022-5320(84)90092-3)
- López, F., R. Delgado, R. López, J. Bacigalupo, and D. Restrepo. 2014. Transduction for pheromones in the main olfactory epithelium is mediated by the Ca^{2+} -activated channel TRPM5. *J. Neurosci.* 34:3268–3278. <https://doi.org/10.1523/JNEUROSCI.4903-13.2014>
- Lowe, G., and G.H. Gold. 1993. Contribution of the ciliary cyclic nucleotide-gated conductance to olfactory transduction in the salamander. *J. Physiol.* 462:175–196. <https://doi.org/10.1113/jphysiol.1993.sp019550>
- Matthews, H.R., and J. Reisert. 2003. Calcium, the two-faced messenger of olfactory transduction and adaptation. *Curr. Opin. Neurobiol.* 4:469–475. [https://doi.org/10.1016/S0959-4388\(03\)00097-7](https://doi.org/10.1016/S0959-4388(03)00097-7)
- Mobley, A.S., A.M. Müller, R.C. Araneda, L.R. Maurer, F. Müller, and C.A. Greer. 2010. Hyperpolarization-activated cyclic nucleotide-gated channels in olfactory sensory neurons regulate axon extension and glomerular formation. *J. Neurosci.* 30:16498–16508. <https://doi.org/10.1523/JNEUROSCI.4225-10.2010>
- Munger, S.D., A.P. Lane, H. Zhong, T. Leinders-Zufall, K.W. Yau, F. Zufall, and R.R. Reed. 2001. Central role of the CNGA4 channel subunit in Ca^{2+} -calmodulin-dependent odor adaptation. *Science*. 294:2172–2175. <https://doi.org/10.1126/science.1063224>
- Nair, K.S., S.M. Hanson, A. Mendez, E.V. Gurevich, M.J. Kennedy, V.I. Sheshtopalov, S.A. Vishnivetskiy, J. Chen, J.B. Hurley, V.V. Gurevich, and V.Z. Slepak. 2005. Light-dependent redistribution of arrestin in vertebrate rods is an energy-independent process governed by protein-protein interactions. *Neuron*. 46:555–567. <https://doi.org/10.1016/j.neuron.2005.03.023>
- Nakashima, N., T.M. Ishii, Y. Bessho, R. Kageyama, and H. Ohmori. 2013. Hyperpolarisation-activated cyclic nucleotide-gated channels regulate the spontaneous firing rate of olfactory receptor neurons and affect glomerular formation in mice. *J. Physiol.* 591:1749–1769. <https://doi.org/10.1113/jphysiol.2012.247361>
- Pietrobon, M., I. Zamparo, M. Maritan, S.A. Franchi, T. Pozzan, and C. Lodovichi. 2011. Interplay among cGMP, cAMP, and Ca^{2+} in living olfactory sensory neurons in vitro and in vivo. *J. Neurosci.* 31:8395–8405. <https://doi.org/10.1523/JNEUROSCI.6722-10.2011>
- Reisert, J., and H.R. Matthews. 1998. Na^+ -dependent Ca^{2+} extrusion governs response recovery in frog olfactory receptor cells. *J. Gen. Physiol.* 112:529–535. <https://doi.org/10.1085/jgp.112.5.529>
- Reisert, J., and H.R. Matthews. 2001. Simultaneous recording of receptor current and intraciliary Ca^{2+} concentration in salamander olfactory receptor cells. *J. Physiol.* 535:637–645. <https://doi.org/10.1111/j.1469-7793.2001.00637.x>
- Reisert, J., and H. Zhao. 2011. Perspectives on: information and coding in mammalian sensory physiology: response kinetics of olfactory receptor neurons and the implications in olfactory coding. *J. Gen. Physiol.* 138:303–310. <https://doi.org/10.1085/jgp.201110645>
- Schild, D., and D. Restrepo. 1998. Transduction mechanisms in vertebrate olfactory receptor cells. *Physiol. Rev.* 78:429–466. <https://doi.org/10.1152/physrev.1998.78.2.429>
- Song, Y., K.D. Cygnar, B. Sagdullaev, M. Valley, S. Hirsh, A. Stephan, J. Reisert, and H. Zhao. 2008. Olfactory CNG channel desensitization by $\text{Ca}^{2+}/\text{CaM}$ via the Bib subunit affects response termination but not sensitivity to recurring stimulation. *Neuron*. 58:374–386. <https://doi.org/10.1016/j.neuron.2008.02.029>
- Stephan, A.B., S. Tobochnik, M. Dibattista, C.M. Wall, J. Reisert, and H. Zhao. 2011. The $\text{Na}^+/\text{Ca}^{2+}$ exchanger NCKX4 governs termination and adaptation of the mammalian olfactory response. *Nat. Neurosci.* 15:131–137. <https://doi.org/10.1038/nn.2943>
- Takeuchi, H., and T. Kurahashi. 2002. Photolysis of caged cyclic AMP in the ciliary cytoplasm of the newt olfactory receptor cell. *J. Physiol.* 541:825–833. <https://doi.org/10.1113/jphysiol.2002.016600>
- Takeuchi, H., and T. Kurahashi. 2003. Identification of second messenger mediating signal transduction in the olfactory receptor cell. *J. Gen. Physiol.* 122:557–567. <https://doi.org/10.1085/jgp.200308911>
- Takeuchi, H., and T. Kurahashi. 2005. Mechanism of signal amplification in the olfactory sensory cilia. *J. Neurosci.* 25:11084–11091. <https://doi.org/10.1523/JNEUROSCI.1931-05.2005>
- Takeuchi, H., and T. Kurahashi. 2008. Distribution, amplification, and summation of cyclic nucleotide sensitivities within single olfactory sensory cilia. *J. Neurosci.* 28:766–775. <https://doi.org/10.1523/JNEUROSCI.3531-07.2008>
- Takeuchi, H., H. Ishida, S. Hikichi, and T. Kurahashi. 2009. Mechanism of olfactory masking in the sensory cilia. *J. Gen. Physiol.* 133:583–601. <https://doi.org/10.1085/jgp.200810085>
- Takeuchi, H., H. Kato, and T. Kurahashi. 2013. 2,4,6-trichloroanisole is a potent suppressor of olfactory signal transduction. *Proc. Natl. Acad. Sci. USA*. 110:16235–16240. <https://doi.org/10.1073/pnas.1300764110>
- Trudeau, M.C., and W.N. Zagotta. 2003. Calcium/calmodulin modulation of olfactory and rod cyclic nucleotide-gated ion channels. *J. Biol. Chem.* 278:18705–18708. <https://doi.org/10.1074/jbc.R300001200>
- Usukura, J., and E. Yamada. 1978. Observations on the cytolemma of the olfactory receptor cell in the newt. 1. Freeze replica analysis. *Cell Tissue Res.* 188:83–98. <https://doi.org/10.1007/BF00220516>
- Wang, J.H. 1952. Tracer-diffusion in liquids. IV. Selfdiffusion of calcium and chloride ion in aqueous calcium chloride solutions. *J. Am. Chem. Soc.* 75:1769–1770. <https://doi.org/10.1021/ja01103a539>